Nuclear Science & Technology Research Institute

Journal of Nuclear Research and Applications

Research Paper

Journal homepage: http://jonra.nstri.ir

Biodistribution and Human Absorbed Dose Evaluation of an Organic-Inorganic Nanocomposite Containing ^{198}Au (^{198}Au/PG4D)

L. Moghaddam Banaem[1], S. Janitabardarzi[1]*, R. Rezaei[2]

[1] Nuclear Fuel Cycle Research School, Nuclear Science and Technology Research Institute, 14155-1339, Tehran, Iran.

[2] Department of biochemistry, Faculty of Science, Zanjan University

(Received: 9 September 2023, Revised: 2 January 2024, Accepted: 6 January 2024)

ABSTRACT

An organic-inorganic nanocomposite ^{198}Au/PG4D was synthesized using polyamidoamine G4 dendrimer and applied as an anticancer agent against 4T1 carcinoma tumor as well as for biodistribution and human absorbed dose investigation. Radionuclide ^{198}Au was produced by irradiation of natural gold (^{197}Au) in a medium flux reactor with 3×10^{11}n/cm^2.s flux of thermal neutron. Gamma spectroscopy exhibited only one characteristic peak of ^{198}Au at 411 KeV as well as a radiochemical purity of more than 82% (using ITLC) was obtained for final formulation of ^{198}Au/PG4D (37MBq). A single intratumor injection of 3.26MBq (88µCi) of ^{198}Au/PG4D resulted in statistically significant 65% growth inhibition in 4T1 tumor volume after 20 days. Biodistribution investigations showed that the tumor had a maximum accommodated activity owing to ^{198}Au/PG4D of 81.27% and 79.37% at 4 and 24 h post injection. The human's absorbed dose, furthermore, was extrapolated via the biokinetics data of mice so that the doses absorbed in the critical organs such as the bone, lung, spleen, kidney, and liver are 0.0669, 1.1, 0.221, 0.0983 and 0.282 mGy/MBq, respectively.

Keywords: ^{198}Au, PG4D, 4T1 cell line, Intratumor injection, Human dosimetry

1. Introductions

Radiotherapy by external or internal irradiation is one of the most powerful manners, however, frequently resulting in disturbance and undesired effect on normal tissues and organs [1]. So, a great deal of research has focused on the internal radiation therapy by intratumor injection of a radiopharmaceutical into the target tumors. Most of beta-emitting radionuclides have been investigated for applying in internal radiation therapy purposes. [2-4]. Some studies have been conducted using the radioactive ^{198}Au for immunoconjugates using colloidal gold nanoparticles range from 1 to several hundred nanometers in size [5]. As ^{198}Au ($t_{1/2}$=2.69 days) decays dominantly by a beta emission (98.99%, 960.7 KeV) and gamma

* Corresponding Author E-mail: sjanitabar@aeoi.org.ir

DOI: https://doi.org/10.24200/jon.2024.1003.

Further distribution of this work must maintain attribution to the author(s) and the published article's title, journal citation, and DOI.

rays (96%, 411 KeV), it is expected to be a suitable radionuclide for suppressing tumor growth and simultaneously ideal matter for tracing the drug in targeting cancer cells [6,7]. It has then reported that the antibody coated gold particles with 40-50 nm diameters against ErbB2 receptors expressed maximal stage of internalization in ErbB2-overexpressing breast cancer cells [8,9]. Nanoparticles with size of almost 100 nm can penetrate into highly permeable tumor walls while, only 30-nm nanoparticles or smaller are able to extravagate and entrance to the poorly permeable tumors to cause distinct therapeutic effect [8].

Many of biomedical dendrimers, on the other hand, are extensively applied as a carrier of colloidal metal thanks to their capability for inhibiting nanoparticles aggregation [10,11]. Polyamidoamine dendrimers (PD) can be applied for these scopes because of possessing a plenty of functional groups appropriate for chelating of metal cations, and interior voids in the structure which make it ideal for hosting small metal components [12]. As the average clinical tumor is only a small fraction of the overall volume and weight of a patient, the tumor acquires a very tiny portion of cardiac output. So, the direct intratumor injection of anticancer agents could be addressed for this problem [13-15]. Taking this observation into account, we came up with some experiments to evaluate the impact of intratumor injection of an organic-inorganic nanocomposite containing ^{198}Au radionuclide on 4T1 tumor. 4T1 breast carcinoma derived from Balb/c mice shares many characteristics with naturally occurring human breast cancer. 4T1 breast carcinoma derived from Balb/c mice shares many characteristics with naturally occurring human breast cancer. The 4T1 tumor is highly tumorigenic and invasive and in contrast to most other tumors, it can spontaneously metastasize from the primary tumor in the mammary gland to multiple distant sites including lymph nodes, liver, blood, brain, lung, and bone [16-17]. So, it can be applicable as a model for studies of anticancer drugs effectiveness [18]. This research includes preparation of a composite by labeling generation four of polyamidoamine dendrimer (PD) with ^{198}Au, study the effect of a single dose delivery of ^{198}Au nanoparticles for treating mice bearing 4T1 carcinoma tumor, biodistribution of ^{198}Au and estimation of human absorbed dose.

2. Experimental

2.1 Materials

PG4D dendrimer was purchased from Sigma-Aldrich. Hydrogen tetracholoroaurate ($HAuCl_4.3H_2O$), sodium borohydride (NaBH4), DMSO (Dimethyl sulfoxide) and sodium hydroxide were received from Merck. RPMI medium 1640, Fetal bovine serum (FBS), gentamicin, penicillin G, streptomycin, trypsin and EDTA were purchased from Gibco. 4T1 mice breast adenocarcinoma cell was obtained from National Cell Bank of Iran Pasteur Institute. The 4T1 cells were cultured and then passaged and finally injected into the mice for creating breast tumors around 3 weeks after injection. For animal anesthesia ketamine and xylazine was purchased from (alfasan Woerden-Holland).

Transmission electron microscopy (TEM, Philips-EM208S) was applied to study the morphology of prepared nanocomposites; besides Gamma spectrometry was performed by liquid scintillation spectrometer model Wallac 1220 Quantulus. Bertold beta counter, Lb123 Model, was used for beta counting. Studies of biodistribution in animals were conducted according to the approving protocols set by the ethical committee of the Radiopharmaceutical Research and Development Lab (RRDL), Nuclear Science and Technology Research Institute of Iran. A high

purity germanium (HPGe) detector which was coupled with a Canberra™ multichannel analyzer (model GC1020-7500SL, Canberra Industries, Inc. CT) and a dose calibrator model ISOMED 1010 were applied for careful determination of distributed activity in different organs of mice. Imaging was prepared via a Siemens camera at 140 keV, with high sensitivity, totally parallel to the collimator after administration of the radio-compound. The distance of the mouse to high energy septa was set to be 12 cm. The useful field of view (UFOV) was 540 mm×400 mm. The spatial resolution was 10 mm FWHM at the CFOV. Sixty-four projections were obtained for 30 seconds per view with a 64×64 matrix.

2.2 Preparation of ^{197}Au/PG4D and ^{198}Au/PG4D nanohybrids

The nano-particle of ^{197}Au/PG4D was prepared according to our previously published article, as well as production of radioactive ^{198}Au/PG4D which was performed under neutron bombardment condition at Tehran Research Reactor as previously reported [19]. Due to the large cross section of ^{197}Au, it captures neutrons efficiently. The samples placed in quartz vials were irradiated by thermal neutron flux of 1×10^{11} n/cm^2.s for 2 h at the Tehran Research Reactor (TRR).

2.3 Quality control

The radionuclidic purity of the synthesized ^{198}Au/PG4D solution was evaluated for the probable presence of other radionuclides using HPGe detector. Radiochemical stability of ^{198}Au/PG4D in final formulation was tested in vitro at pH~7.5 and at the following time points: 2, 8, 24 and 48h. The stability was evaluated in fresh human serum and PBS by instant thin layer chromatography (ITLC) method. In these experiments, a 70:30 of methanol-water mixture was chosen as the mobile phase and number 1 Whatman cellulose paper as the stationary phase. 100µL(37MBq) of the ^{198}Au/PG4D was poured into the human blood serum and PBS (phosphate buffered saline) and incubated at 37 °C. Thereafter the proportion of free ^{198}Au to ^{198}Au/PG4D was determined [19, 20, 21].

2.4 Tumor inoculation and in vivo study

0.1 mL serum free medium 4T1 breast cancer cell solution was subcutaneously injected in the left flank female Balb/c mice with almost 10^5–10^6 cells. The nodules of 95% of tumor bearing mice reached a volume of 589 ± 50 mm^3 after approximately 3 weeks. After that, the tumor bearing mice were divided into 4 groups and used for the in vivo survey as follows: Group 1: PBS treated group with 5 mice; Group 2: ^{197}Au/PG4D treated group by intratumor injection with 3 mice, and Group 3: ^{198}Au/PG4D treated group by intratumor injection with 6 mice. The test animals of group 3 were received a single injection of ^{198}Au/PG4D into the tumor. The mice in group 3 were divided into two distinct group, with 3 members in each, for conducting two different tests including tumor volume determination versus time, and pharmacokinetics evaluation purposes. All the mice were weighed and numbered before the treatment and their initial tumor volumes were recorded. The control animals, however, received an injection of 100 µL of PBS. The tumor volume of 3 mice was evaluated over a period of 20 days for each mouse. The width and length of tumors were determined via a digital caliper and then evaluated according to 0.4 ($L\times W^2$) formula; where L and W are length and width, respectively [22,23]. Another group included of 3 tumor bearing mice, treated with single dose of ^{198}Au/PG4D, was tested to evaluate the pharmacokinetics distribution of ^{198}Au/PG4D nanocomposite in critical organs of them.

We conducted another study on a group including 3 normal mice treated by ^{198}Au/PG4D

via intravenous injection for evaluation the pharmacokinetics and extrapolation to human data. In the latest group, all of 3 normal mice were undergone scarification at prearranged times 4h, 24h and 48h post injection in order to obtain dosimetry data. The amount of absorbed activity in the different tissues were counted with a γ-ray scintillation. The lungs, heart, spleen, liver, kidneys, intestine, femur and the muscles surrounding the femur were dissected, weighed and counted.

2.5 Statistics

All the tests were repeated three times and data was presented as the mean ±SD. Statistical surveys were drawn by applying a three and four-way analyses of variance ANOVA with post hoc testing to compare Sidak tests. Pair-wise comparisons between treatments were made via independent sample t-test, IBM SPSS Statistic 23, using Microsoft Excel. A p-Value of < 0.05 was contemplated statistically significant.

2.6 Dosimetry

The estimated human absorbed dose was calculated using the mass correction approach (kg/g method) [24] and its evaluation was performed by the extrapolation of animal biodistribution data to humans [24]. The animal data were obtained by intravenous injection to 3 normal mice. The biodistributions were assessed during 4h, 24h, and 48h time intervals. On the other side, the 73kg mass information for the typical adult male was taken from ICRP89 [25]. Based on the %ID as a function of time for each ex-studied part of body, the time-integrated activity coefficients (τ) (Bq-h/Bq) and the cumulative activities in source organs are calculated [26]. Finally, the absorbed doses of human organs were calculated in accordance with the MIRD recommended approach using the Matlab software, MIRDOSE program along with the S-values of ^{198}Au and predicted time-integrated activity coefficients(τ), [27]. The followings were considered as the MIRDOSE software's source organs: the liver, kidney, bone, spleen, muscle, and red blood cells. The activity accumulated in the bone was assumed to partition between cortical and trabecular bone equally.

3. Results and discussion

3.1 Quality control of ^{198}Au/PG4D nanocomposite

The radionuclidic purity of the ^{198}Au/PG4D nanocomposite was examined by beta and gamma spectroscopy. The beta specrtoscopy was performed at different time intervals for evaluation of the decay constant to assure the revealed peak was related to the ^{198}Au (Fig. 1). It was illustrated that the sole beta energy peak is around 137KeV that is one third of maximum energy of ^{198}Au beta emission. As it can be seen in Fig.1 there is a deviation in the spectrum during the passing time of measurment that is due to the reduction of constant leading term for the transition and energy-dependent terms are not negligible any longer. This finding is in accordance with the data reported by D. Parsignault [28].

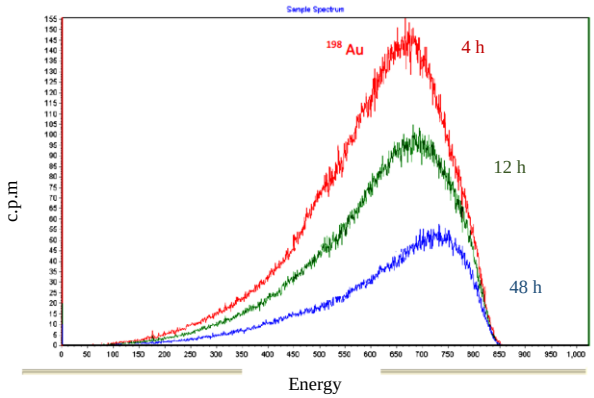

Fig. 1. Beta spectroscopy of ^{198}Au/PG4D nanocomposite and inset: its gamma spectroscopy data.

The HPGe spectrum of radioactive ^{198}Au presented at inset of Fig. 1 revealed a peak at 411.8 KeV (23.35 ± 0.41 Bq/cc). According to the literatures, ^{199}Au (t1/2 = 3.2 days) exhibits two characteristic gamma peaks at about 208 and 158 KeV [6, 26]. As revealed in the inset, the

presented spectrum showed no remarkable emissions except than the 411.8KeV, which is attributed to ^{198}Au. ^{199}Au can be produced by double neutron capture on ^{197}Au targets; yet in the TRR reactor, utilized in this research, owing to the low flux of neutron, the possibility of ^{199}Au production is too low so that it cannot be detected. Hence, absence of ^{199}Au and other radionuclides would be authenticated by this analysis.

TEM analyses of nanoparticles (Fig. 2) conducted to perceive the size and morphology of particles revealed spherical shape for both of ^{198}Au/PG4D and ^{197}Au/PG4D composites. ^{197}Au/PG4D, however, has shown smaller particle size compared to ^{198}Au/PG4D. This could be attributed to partial polymerization of PG4D owing to bombardment with neutron.

Radiochemical stability of ^{198}Au-nanoparticles at time intervals 2, 8, 24 and 48 h was evaluated at 37°C by means of ITLC in PBS and human serum which are shown in Fig. 3.

The ^{198}Au/PG4D stability in PBS and serum after 2h were determined to be 93.25±6.23% and 96.58±3.54%, respectively. However, after 48h, it decreased to 81.32±2.35% in the PBS, and to 82.78±6.87% in the human serum samples. In general, stability decreases over the time that could be attributed to protein interactions such as albumin in the serum [29–31].

3. 2 In vivo anticancer efficacy of ^{197}Au/PG4D and ^{198}Au/PG4D targeted nanoparticles

The growth rate of 4T1 breast tumors versus time after treatment with one dose of radioactive ^{198}Au/PG4D, non-radioactive ^{197}Au/PG4D nanocomposites and PBS is shown in Fig. 4. Experiments illustrated that non-radioactive ^{197}Au/PG4D (3.17×10^{-7} mol) has no significant inhibitory effect on tumor growth in comparison with the group treated by PBS.

As shown in Fig. 4, the radioactive ^{198}Au/PG4D (3.26MBq) exhibited superior antitumor effect in comparison with the non-radioactive ^{197}Au/PG4D. Not only was no remarkable increment of tumor volume observed in the mice treated with ^{198}Au/PG4D from day 0 to 20 of post injection ($p < 0.05$), the volume vividly underwent a decrement at day 6 measurement. The mean tumor volume during 6 days in the ^{198}Au/PG4D, ^{197}Au/PG4D and PBS

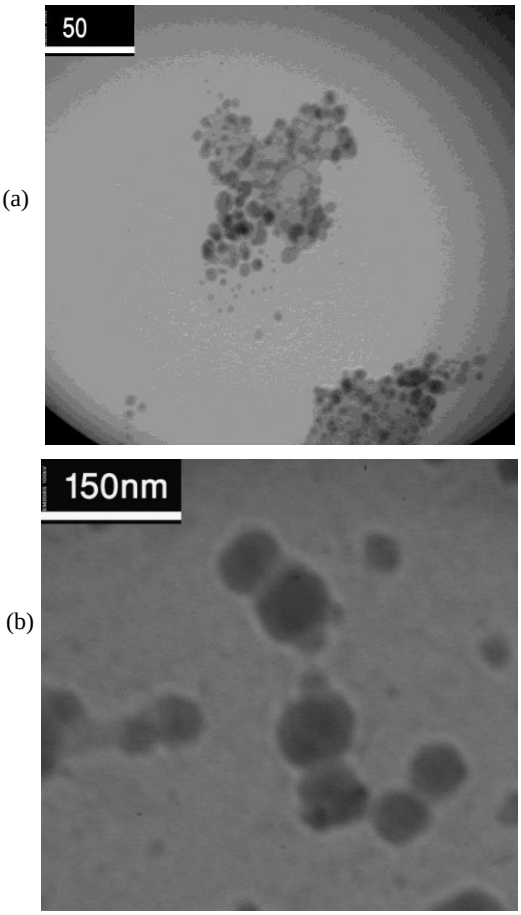

Fig. 2. TEM photos of ^{197}Au/ PG4D (a) and ^{198}Au/ PG4D materials (b) [19].

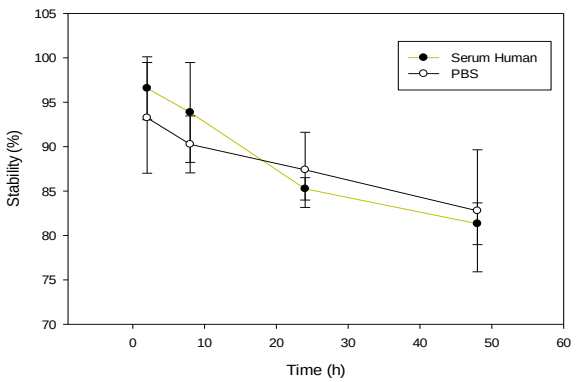

Fig. 3. PBS and serum stability of ^{198}Au/PG4D radiolabeled composite at various time intervals.

treated groups were 464.01, 795.01 and 789.12 mm^3, respectively. Furthermore, on the 20th day, the mean tumor volume in the ^{198}Au/PG4D, ^{197}Au/PG4D and PBS treated groups were 636.11, 1606.89 and 1829.12 mm^3, respectively. The tumor volume of the mice, received ^{198}Au/PG4D, was suppressed significantly compared to tumor volume in the non-radioactive ^{197}Au/PG4D treated group 20 days after treatment.

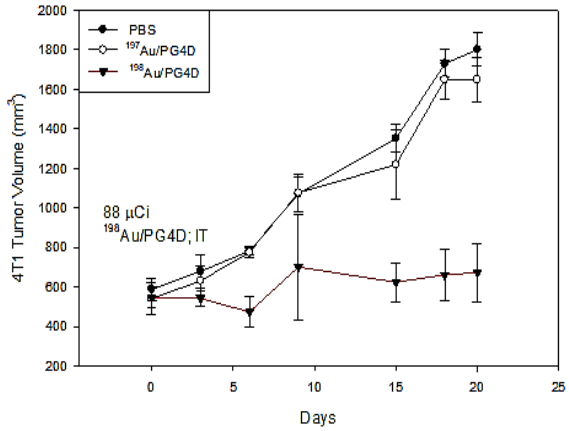

Fig. 4. Change of tumor volume versus time in the 4T1 cancer bearing Balb/c mice recived intratumoral injection of ^{197}Au/PG4D, ^{198}Au/PG4D and PBS at day 0 of study.

According to Table 1, the ^{197}Au/PG4D treated group showed a bit more gentle tumor growth in comparison with the PBS treated group, however, the discrepancy was not statistically significant (P = 0.804). In the case of ^{198}Au/PG4D treated group, a statistically significant (P = 0.001) decrease of tumor growth of over 65% was observed. These results illustrate that the 3.26MBq (88µCi) radiation carried by ^{198}Au/PG4D nanocomposite directly into the tumor was adequate to meaningfully inhibit the tumor growth thanks to the radioactive dose, rather than probable toxicity of the non-radioactive ^{197}Au/PG4D compound.

Fig. 5 represents the percentage of absorbed dose per gram of organs in the tumor bearing mice at different time post injection of 3.26MBq (88µCi) of ^{198}Au/PG4D labeled nanocomposite. Biodistribution studies revealed that the retention of compound at the tumor up to 24h post injection is remarkable. The average particle size of the ^{198}Au/PG4D, about 60 nm, is suitable enough to potentially enable passive accumulation in the tumor via the known enhanced permeation and retention (EPR) effect [28, 31]. In the case of probable leak from the tumor, the injected ^{198}Au/PG4D labeled nanocomposite would specially accumulate in the reticuloendothelial (RE) system. According to Fig. 5, ^{198}Au/PG4D evades the capture of reticuloendothelial system and the activity observed different organs such as spleen and lung and is low too. It reveals that the amounts of leak of nanocomposite to these organs are low.

Table 1. Changes in growth rates between the days 0 and 20 as mixed procedure, SE: standard error; DF: degrees of freedom from independent sample t-test.

Experiment	DF	Mean± SE	t- Value	p- Value
PBS vs. ^{198}Au/PG4D (3.26MBq)	54	672.82±36	5.232	0.001
PBS vs. ^{197}Au/PG4D	54	33.35±38.11	0.213	0.804
^{197}Au/PG4D vs. ^{198}Au/PG4D (3.26MBq)	40	639.45±34.19	5.788	0.001

The ɣ-biodistribution of ^{198}Au/PG4D in the tumor bearing Balb/c mice was also studied by SPECT imaging. The inset of Fig. 5 shows the incidence images of mice bearing tumor right 4h and 24h after injection. After ^{198}Au/PG4D 3.26MBq (88µCi) injection in tumor, due to the decay of ^{198}Au by gamma emission, imaging opportunity for detecting the injection site

activity is available. As shown in Fig. 5, the ^{198}Au/G4D complex is majorly accumulated at the injection site and no significant leaks are observed even 24 h post injection. This result is in accordance with ^{198}Au/PG4D biodistribution results presented in the inset of Fig 5. It could be due to successful accumulation of radioactive nanocomposite in the tumors via the known EPR effect. At the end, animal was anesthetized by intra-peritoneal injection of Ketamine and Xylazine (65 and 13 mg/kg). The biodistribution is in accordance with other radiopharmaceuticals that used PG4D for labeling [32, 33].

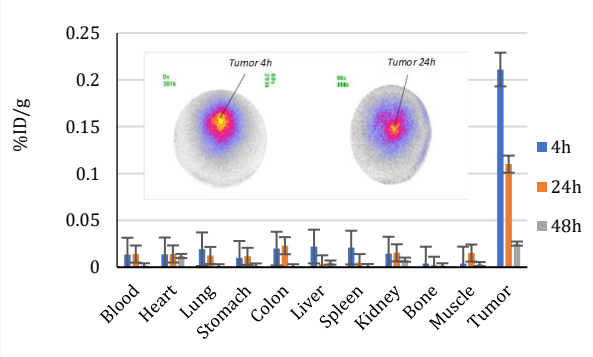

Fig. 5. Distribution of ^{198}Au/PG4D in different organs of tumor bearing Balb/c mice, 4h, 24h and 48h after tumor injection (n=3)- inset: incidence images of tumor of Balb/c mice 4h and 24h after tumor injection.

3.3 Dosimetry

Implementing the estimated percentage of the injected activity (%ID) for human, the time-integrated activity coefficients and cumulated activities of source organs were determined by MIRD schema, non-linear regression analysis and MATLAB software [25]. The calculated %ID for humans from extrapolation of %ID/g data of mice and obtained human absorbed dose from ^{198}Au/PG4D by MIRD schema have been shown in Fig. 6 and Fig. 7. The estimated time-integrated activity coefficients and human absorbed dose of ^{198}Au/PG4D by also were presented in Table 2.

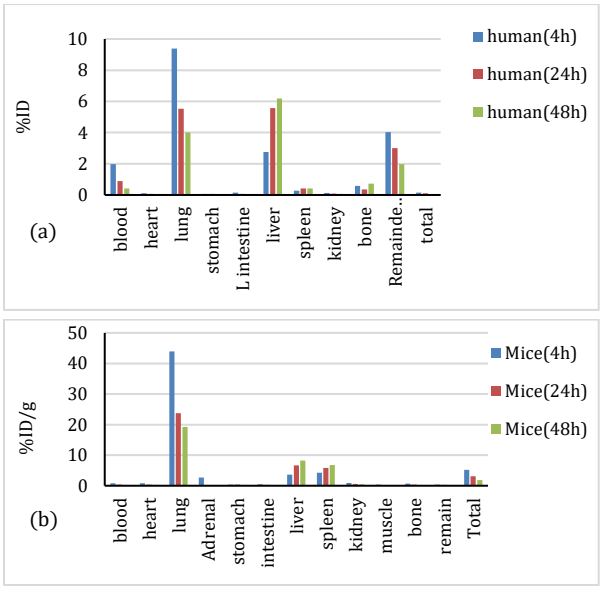

Fig. 6. (a) Biodistribution of labelled nanocomposite in the mice at 4h, 24h and 48h after injection, (b) Human's %ID/organ extrapolated from %ID/g of mice.

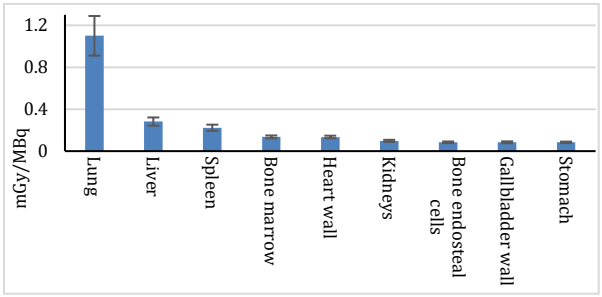

Fig. 7. The obtained human absorbed dose from ^{198}Au/PG4D using MIRD schema.

After the residence time estimation, they were applied to obtain the absorbed doses of organs using MIRDOSE schema and the data is presented in Table 2. It can be seen in Table 2 that the absorbed dose in sensitive organs like the spleen, liver, bone, red marrow, and kidney are 0.221, 0.282, 0.0669, 0.125 and 0.0983 mGy/MBq, respectively.

A good number of previous works revealed that permeation of gold nanoparticles is a size dependent phenomenon [34-36]. Sonavane et al. evaluated the biological distribution of differently size gold nanoparticles (NP) up on intravenous administration in mice. According to Sonavane research, In the case of 15, 50 and 100 nm size gold nanoparticles stabilized with biodegradable/biocompatible stabilizer, higher

accumulation of gold was observed in liver, lung and spleen and trace amount was observed in organs like brain, heart, kidney, pancreas and stomach. In case of 200 nm size gold NP, highest concentration of gold was observed in the liver followed by spleen lung and kidney.

Table 2. Estimated coefficients of time-integrated activity and human absorbed dose of ^{198}Au/PG4D by MIRD schema.

Organs	coefficients of time-integrated activity (Hour)	Absorbed dose (mGy/MBq)
Blood	2.62	-
Heart	0.05	1.32E-01
Lung	5.83	1.10E+00
Stomach	0.034	8.40E-02
L intestine	0.108	5.68E-2
Liver	2.297	2.82E-01
Spleen	0.173	2.21E-01
Kidney	0.091	9.83E-02
Bone	1.020	6.69E-02
Red Marrow	0.94	1.25E-01
Remainder	2.497	-
Total Body	2.069	5.94E-2
EFF DOSE EQUIV	-	1.96E-01 mSv/MBq
EFF DOSE	-	2.16E-01 mSv/MBq

Similar to earlier observations about gold nanocomposites, ^{198}Au/PG4D with the highest population of particle size at about 60 nm also showed high level of gold concentration in the in lung, liver, and in the next spleen whilst, trace amount was seen in other organs (fig. 6). In our present study, the obtained results were in congruence with Sonavane findings. There is a list of factors that can influence nanoparticle-cell interactions at the nano-bio interface including size, shape, charge of nanoparticle, ligand density, Receptor expression levels, Internalization mechanism and cell properties (phenotype, location) [37]. However, there is still debate as to whether the rapid accumulation in the liver and lung is due to simple filtration or increased binding opportunities between the mononuclear phagocyte system (MPS) cells and the nanoparticles [38].

4. Conclusion

In the present study, a radioactive organic-inorganic nanocomposite (^{198}Au/PG4D) was prepared and its inhibitory effect against the growth of 4T1 cancer cells was evaluated in comparison with non-radioactive ^{197}Au/PG4D. Moreover, the suitability of the prepared radioactive compound for tumor treatment following intratumoral injection was evaluated in tumor-bearing BALB/c mice. A single dose of 3.26MBq (88μCi) radioactive ^{198}Au/PG4D nanocomposite in normal saline, directly injected into the mice 4T1 breast cancer tumors, brought about a statistically significant reduction of tumor growth rate within a short time frame. This study, hence, discloses the fact that radioactive ^{198}Au/PG4D nanohybrid can deliver curable doses to tumors along with the evidence for good in vivo tolerance makes these particles ideal candidates for future medical applications. The estimation of absorbed dose by human organs from ^{198}Au by ^{198}Au/PG4D nanocomposite by vein injection for vital organs was performed and reveals that further preclinical evaluation must be performed to estimate the dosimetry, toxicity, as well as biokinetics of this radiopharmaceutical.

References

1. Seong SK, Ryu JM, Shin DH, Bae EJ, Shigematsu A, Hatori Y, et al. Biodistribution and excretion of radioactivity after the administration of 166Ho-chitosan complex (DW-166HC) into the prostate of rat. European journal of nuclear medicine and molecular imaging. 2005;32(8):910-7.
2. Song H-C, Kun N, Park K-H, Shin C-H, Bom H-S, DONGMIN K, et al. Intratumoral administration of rhenium-188-labeled pullulan acetate nanoparticles (PAN) in mice bearing CT-26 cancer cells for suppression of tumor growth. Journal of microbiology and biotechnology. 2006;16(10):1491-8.
3. Bakker RC, Lam M, Nimwegen SAV, Rosenberg AJWP, Es RJJ, Nijsen JFW. Journal of Radiation Oncology, 6 323 (2017).
4. Lee I, Lee YH. The effect of various therapeutic solutions including colloidal chromic 32P via an

intratumoral injection on the tumor physiological parameters of AsPC-1 human pancreatic tumor xenografts in nude mice. Clinical Cancer Research. 1999;5(10):3139s-42s.
5. Khan MK, Minc LD, Nigavekar SS, Kariapper MS, Nair BM, Schipper M, et al. Fabrication of {198 Au 0} radioactive composite nanodevices and their use for nanobrachytherapy. Nanomedicine: Nanotechnology, Biology and Medicine. 2008;4(1):57-69.
6. K.C. Black, et al., ACS Nano, 8 4385 (2014).
7. Rezaei R, Darzi SJ, Yazdani M, Anti cancer Agents Med Chem, 20 1250 (2020).
8. Durymanov MO, Rosenkranz AA, Sobolev AS. Current approaches for improving intratumoral accumulation and distribution of nanomedicines. Theranostics. 2015;5(9):1007.
9. Jiang W, Kim BY, Rutka JT, Chan WC. Nanoparticle-mediated cellular response is size-dependent. Nature nanotechnology. 2008;3(3):145-50.
10. Narmani A, Arani MA, Mohammadnejad J, Vaziri AZ, Solymani S, Yavari K, Talebi F, Darzi SJ. Breast tumor targeting with PAMAM-PEG-5FU-99m Tc as a new therapeutic nanocomplex: in in-vitro and in-vivo studies. Biomedical Microdevices. 2020 Jun;22:1-3.
11. Han H, Xing J, Chen W, Jia J, Li Q. Fluorinated polyamidoamine dendrimer-mediated miR-23b delivery for the treatment of experimental rheumatoid arthritis in rats. Nature Communications. 2023 Feb 20;14(1):944.
12. Ernandes T, Daniel-da-Silva AL, Trindade T. Metal-dendrimer hybrid nanomaterials for sensing applications. Coordination Chemistry Reviews. 2022 Jun 1;460:214483.
13. Walter KA, Tamargo RJ, Olivi A, Burger PC, Brem H. Intratumoral chemotherapy. Neurosurgery. 1995;37(6):1129-45.
14. Voulgaris S, Partheni M, Karamouzis M, Dimopoulos P, Papadakis N, Kalofonos HP. Intratumoral doxorubicin in patients with malignant brain gliomas. American journal of clinical oncology. 2002 Feb 1;25(1):60-4.
15. Lammers T, Peschke P, Kühnlein R, Subr V, Ulbrich K, Huber P, et al. Effect of intratumoral injection on the biodistribution, the therapeutic potential of HPMA copolymer-based drug delivery systems. Neoplasia. 2006;8(10):788-95.
16. Pulaski BA, Terman DS, Khan S, Muller E, Ostrand-Rosenberg S. Cooperativity of Staphylococcal aureus enterotoxin B superantigen, major histocompatibility complex class II, and CD80 for immunotherapy of advanced spontaneous metastases in a clinically relevant postoperative mouse breast cancer model. Cancer research. 2000;60(10):2710-5.
17. Tao K, Fang M, Alroy J, Sahagian GG. Imagable 4T1 model for the study of late stage breast cancer. BMC cancer. 2008;8(1):228.
18. Heppner GH, Miller FR, Shekhar PM. Nontransgenic models of breast cancer. Breast Cancer Research. 2000;2(5):331.
19. Janitabar-Darzi S, Rezaei R, Yavari K. In vitro Cytotoxicity Effects of 197Au/PAMAMG4 and 198Au/PAMAMG4 Nanocomposites Against MCF7 and 4T1 Breast Cancer Cell Lines. Advanced pharmaceutical bulletin. 2017;7(1):87.
20. Balogh L, Ganser T, Shi X, editors. Characterization of dendrimer-gold nanocomposite materials. Materials Research Society Symposium Proceedings; 2005: Warrendale, Pa.; Materials Research Society; 1999.
21. Garcia ME, Baker LA, Crooks RM. Preparation and characterization of dendrimer− gold colloid nanocomposites. Analytical chemistry. 1999 Jan 1;71(1):256-8.
22. Vredenburg MR, Ojima I, Veith J, Pera P, Kee K, Cabral F, et al. Effects of orally active taxanes on P-glycoprotein modulation and colon and breast carcinoma drug resistance. Journal of the National Cancer Institute. 2001;93(16):1234-45.
23. Wang P, Zhao X-H, Wang Z-Y, Meng M, Li X, Ning Q. Generation 4 polyamidoamine dendrimers is a novel candidate of nano-carrier for gene delivery agents in breast cancer treatment. Cancer letters. 2010;298(1):34-49.
24. Fathi F, Moghaddam-Banaem L, Shamsaei M, Samani A, Maragheh MG. Production, biodistribution, and dosimetry of 47Sc-1, 4, 7, 10-tetraazacyclododecane-1, 4, 7, 10-tetramethylene phosphonic acid as a bone-seeking radiopharmaceutical. Journal of Medical Physics/Association of Medical Physicists of India. 2015 Jul;40(3):156.
25. Valentin J. Basic anatomical and physiological data for use in radiological protection: reference values: ICRP Publication 89. Annals of the ICRP. 2002;32(3):1-277.
26. Deilami-nezhad L, Moghaddam-Banaem L, Sadeghi M. Development of bone seeker radiopharmaceuticals by Scandium-47 and estimation of human absorbed dose. Applied radiation and isotopes. 2017;129:108-16.
27. Siegel JA, Thomas SR, Stubbs JB, Stabin MG. MIRD pamphlet no. 16: techniques for quantitative radiopharmaceutical biodistribution data acquisition and analysis for use in human radiation dose estimates. The Journal of Nuclear Medicine. 1999;40(2):37S.
28. Parsignault D. The Beta Spectrum of Au198, and the Conversion Coefficients of the 412-keV Line

in Hg198. In Internal Conversion Processes 1966 Jan 1 (pp. 173-182). Academic Press.
29. Tang MX, Redemann CT, Szoka FC. In vitro gene delivery by degraded polyamidoamine dendrimers. Bioconjugate chemistry. 1996;7(6):703-14.
30. Yuv S, Eyu G, Av S, Aa L, Iyu K, Nv P, Mi L. Experimental study of dendrimer-based nanoparticles with RGD-peptide for anticancer radionuclide therapy. Bulletin of Russian State Medical University. 2018(6):113-9.
31. Liu H, Xu Y, Wen S, Chen Q, Zheng L, Shen M, et al. Targeted tumor computed tomography imaging using low-generation dendrimer-stabilized gold nanoparticles. Chemistry–A European Journal. 2013;19(20):6409-16.
32. Aghaei-Amirkhizi N, Moghaddam-Banaem L, Athari-Allaf M, Sadjadi S, Johari-Daha F. Development of dendrimer encapsulated Radio-Ytterbium and biodistributionin tumor bearing mice. IEEE Transactions on NanoBioscience. 2016 Jul 7;15(6):549-54.
33. Moghaddam-Banaem L, Amirkhizi NA, Sadjadi S, Johari-Deha F, Athari-Allaf M. The Preparation, Biodistribution, and Dosimetry of Encapsulated Radio-Scandium in a Dendrimer for Radio-nano-pharmaceutical Application. Iranian Journal of Pharmaceutical Research. 2022 Dec 31;21(1).
34. Sonavane G, Tomoda K, Sano A, Ohshima H, Terada H, Makino K. In vitro permeation of gold nanoparticles through rat skin and rat intestine: effect of particle size. Colloids and Surfaces B: Biointerfaces. 2008 Aug 1;65(1):1-0.
35. Sonavane G, Tomoda K, Makino K. Biodistribution of colloidal gold nanoparticles after intravenous administration: effect of particle size. Colloids and Surfaces B: Biointerfaces. 2008 Oct 15;66(2):274-80.
36. T. Niidome, M. Yamagata, Y. Okamoto, Y. Akiyama, H. Takahashi, T. Kawano, Y. Katayama, Y. Niidome, Journal of Control Release 114 343 (2006).
37. Moghaddam-Banaem L, Janitabar-Darzi S, Rezaei R. Biodistribution and human absorbed dose evaluation of an organic-inorganic nanocomposite containing 198 Au (198 Au/PG4D), JONRA.
38. Owens III DE, Peppas NA. Opsonization, biodistribution, and pharmacokinetics of polymeric nanoparticles. International journal of pharmaceutics. 2006 Jan 3;307(1):93-102.

How to cite this article

L. Moghaddam Banaem, S. Janitabardarzi, R. Rezaei, *Biodistribution and Human Absorbed Dose Evaluation of an Organic-Inorganic Nanocomposite Containing 198Au (198Au/PG4D)*, Journal of Nuclear Science and Applications (JONRA) Volume 4 Number 1 Winter (2024) 35-44.
URL: https://jonra.nstri.ir/article_1621.html**, DOI**: https://doi.org/10.24200/jon.2024.1003.

This work is licensed under the Creative Commons Attribution 4.0 International License.
To view a copy of this license, visit http://creativecommons.org/licenses/by/4.0